Polymer Journal (2019) 51:461–470
https://doi.org/10.1038/s41428-018-0165-0

ORIGINAL ARTICLE

Biobased polymer networks by the thiol-ene photopolymerization of allylated *p*-coumaric and caffeic acids

Mitsuhiro Shibata[1] · Kaito Sugane[1] · Yuto Yanagisawa[1]

Received: 19 October 2018 / Revised: 4 December 2018 / Accepted: 10 December 2018 / Published online: 8 January 2019

Abstract

Diallylated *p*-coumaric acid (A2CM) and triallylated caffeic acid (A3CF) were synthesized by the reactions of *p*-coumaric acid and caffeic acid with allyl bromide in the presence of potassium carbonate. The thiol-ene photopolymerization of A2CM and a pentaerythritol-based tetrathiol (S4P) as well as that of A3CF/S4P at allyl/thiol and (allyl + enone)/thiol ratios of 1/1 produced cured products. The FT-IR spectral analysis revealed that the thiol-ene reaction of allyl and thiol groups mainly progressed for the products cured at an allyl/thiol ratio of 1/1, while both allyl and enone groups reacted with thiol groups for the products cured at an (allyl + enone)/thiol ratio of 1/1. The progress of the thiol-ene reaction of the enone and thiol groups caused the lowering of the glass transition and 5% weight loss temperatures (T_g and T_{d5}). The A3CF/S4P cured at an allyl/thiol ratio of 1/1 exhibited the highest T_g, T_{d5}, tensile strength, and tensile modulus among all the cured products.

Introduction

The utilization of renewable resources to replace petroleum as a limited resource in polymer synthesis has been a subject of substantial recent interest in academia and industry [1–5]. Thiol-ene photopolymerization from renewable resources is well-suited for the production of biobased polymer networks with various frameworks and functional groups due to many advantageous features such as solvent-free conditions, a lack of water and oxygen sensitivities, a high conversion and yield, a lack of byproducts, and rapid reaction rates [6–10]. In past studies, biobased polymer networks have been prepared by thiol-ene photopolymerization utilizing renewable nonaromatic resources such as vegetable oils [11–14], carbohydrates [15–18], terpenes [19, 20], and amino acids [21, 22]. As other renewable resources, the phenolic compounds that occur universally in the plant kingdom are promising renewable resources for the production of thiol-ene polymer networks, as the phenolic hydroxy groups can be easily converted to alkenyloxy groups, and the stable and rigid aromatic rings impart excellent thermal and mechanical properties. For example, our research group reported biobased polymer networks by the thiol-ene photopolymerization of allylated or acrylated derivatives of eugenol [23, 24], gallic acid and pyrogallol [25] with various polythiol compounds. Yang et al. reported biobased thiol-ene networks utilizing allylated compounds of hydroxybenzoic acids [26], gentistic acid and gallic acid [27]. Hydroxycinnamic acids are promising candidates for the production of biobased thiol-ene networks because the central unsaturated carbonyl (enone) group can undergo the thiol-ene reaction. However, these studies have not yet been reported to the best of our knowledge. In this study, we used *p*-coumaric acid (CMA) and caffeic acid (CFA), which are widely distributed in fruits, vegetables and mushrooms [28]. CMA is mainly biosynthesized from cinnamic acid and L-tyrosine by the action of a cinnamate 4-monooxygenase and tyrosine ammonia lyase, respectively [29, 30]. CFA is biosynthesized by the hydroxylation of CMA using a 4-coumarate 3-hydroxylase (C3H) or bacterial cytochrome P450 monooxygenase [30, 31]. Although CMA and CFA are slightly more expensive than comparable reagents, it is known that their derivatives have various biological activities such as antioxidant, anti-inflammatory, antibacterial, antiviral and

Supplementary information The online version of this article (https://doi.org/10.1038/s41428-018-0165-0) contains supplementary material, which is available to authorized users.

✉ Mitsuhiro Shibata
mitsuhiro.shibata@p.chibakoudai.jp

[1] Department of Life and Environmental Sciences, Faculty of Engineering, Chiba Institute of Technology, 2-17-1 Tsudanuma, Narashino, Chiba 275-0016, Japan

antitumor activities [28, 32]. In this study, diallylated coumaric acid (A2CM) and triallylated caffeic acid were synthesized by the allylation of CMA and CFA, respectively (Scheme 1), and the thermal and mechanical properties of their photocured products with pentaerythritol tetrakis (3-mercaptopropionate) (S4P) at different molar ratios were investigated. In these photocuring compounds, the thiol-ene reaction of allyl and thiol groups [22–24], thiol-ene reaction of enone and thiol groups [9], and [2 + 2] photodimerization of cinnamoyl moieties [33, 34] are considered as probable curing reactions (Scheme 2). The purpose of this work is to elucidate the influence of the feed molar ratios of A2CM/S4P and A3CF/S4P on the three types of curing reactions and the thermomechanical properties of the cured products, with the aim of developing bioactive coating materials whose properties can be controlled by changing the molar ratio of monomers and curing conditions.

Materials and methods

Materials

Coumaric acid (CMA), caffeic acid (CFA), allyl bromide, and potassium carbonate were purchased from Kanto Chemical Co., Inc. (Tokyo, Japan). The pentaerythritol-based tetrathiol (S4P) was purchased from Sigma-Aldrich Corporation (St. Louis, MO, USA). *N*,*N*-Dimethylformamide (DMF) was purchased from Wako Pure Chemical Industries, Ltd. (Osaka, Japan). As photoinitiators, 1-hydroxycyclohexyl phenyl ketone (IRGACURE® 184, mp. 45–49 °C, ultraviolet (UV)/visible (VIS) absorption peaks in methanol: 246, 280,and 333 nm) and phenyl bis(2,4,6-trimethylbenzoyl)phosphine oxide (IRGACURE® 819, mp. 127–133 °C, UV/VIS absorption peaks in methanol: 295 and 370 nm) were purchased from Toyotsu Chemiplas Corporation (Tokyo, Japan). All of the commercially available reagents were used without further purification.

Preparation of diallylated coumaric acid (A2CM)

Potassium carbonate (27.6 g, 200 mmol) was added to a solution of CMA (8.21 g, 50.0 mmol) in DMF (150 mL), and the resulting mixture was stirred for 10 min. Allyl bromide (24.2 g, 200 mmol) was dropwise added over a period of 30 min at room temperature. After the addition, the mixture was stirred for 24 h at 40 °C and filtered. Dilute hydrochloric acid was added to the filtrate, and the product was extracted with ethyl acetate/hexane 3/1 (v/v, 50 mL ×3) three times. The organic layer was washed with water, dried over sodium sulfate and concentrated in vacuo to produce a mixture of incompletely allylated compounds (7.8 g) as a pale yellow liquid. The isolated crude product was again reacted with allyl bromide (3.63 g, 30.0 mmol) and potassium carbonate (4.14 g, 30.0 mmol) in a similar manner to the above to give A2CM as a pale yellow liquid (6.34 g) in 52% yield. A2CM: ^{13}C-NMR (100 MHz, δ, ppm, in $CDCl_3$) 166.57 (C-1), 160.58 (C-7), 144.99 (C-3), 133.59 (C-11,14), 130.64 (C-5, 9), 127.19 (C-4), 118.82, 118.23, 118.15 (C-2, 12, 15), 115.61, 115.52 (C-6, 8), 68.55 (C-13), 64.81 (C-10); ESI-MS (positive mode, *m/z*) calcd. for $C_{15}H_{16}O_3$ 244.1100, found $[M + H]^+$ 245.1170.

Preparation of triallylated caffeic acid (A3CF)

Potassium carbonate (34.6 g, 250 mmol) was added to a solution of CFA (9.01 g, 50.0 mmol) in DMF (150 mL), and the resulting mixture was stirred for 10 min. Allyl bromide (30.2 g, 250 mmol) was dropwise added over a period of 30 min at room temperature. After the addition, the mixture was stirred for 24 h at 40 °C and filtered. Dilute hydrochloric acid was added to the filtrate, and the product was extracted with ethyl acetate/hexane 3/1 (v/v, 50 mL ×3) three times. The organic layer was washed with water, dried over sodium sulfate and concentrated in vacuo to produce a mixture of incompletely allylated compounds (9.1 g) as a pale yellow liquid. The isolated crude product was again reacted with allyl

Scheme 1 Synthesis of A2CM and A3CF

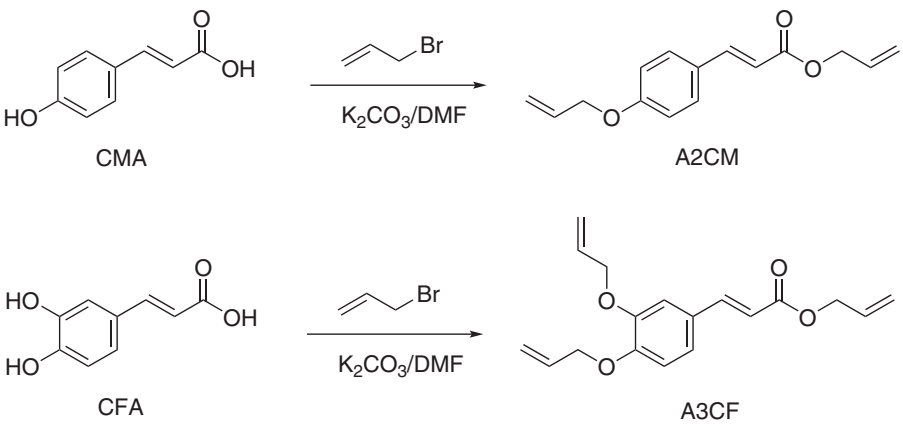

Scheme 2 Chemical structure of S4P and probable photocuring reactions

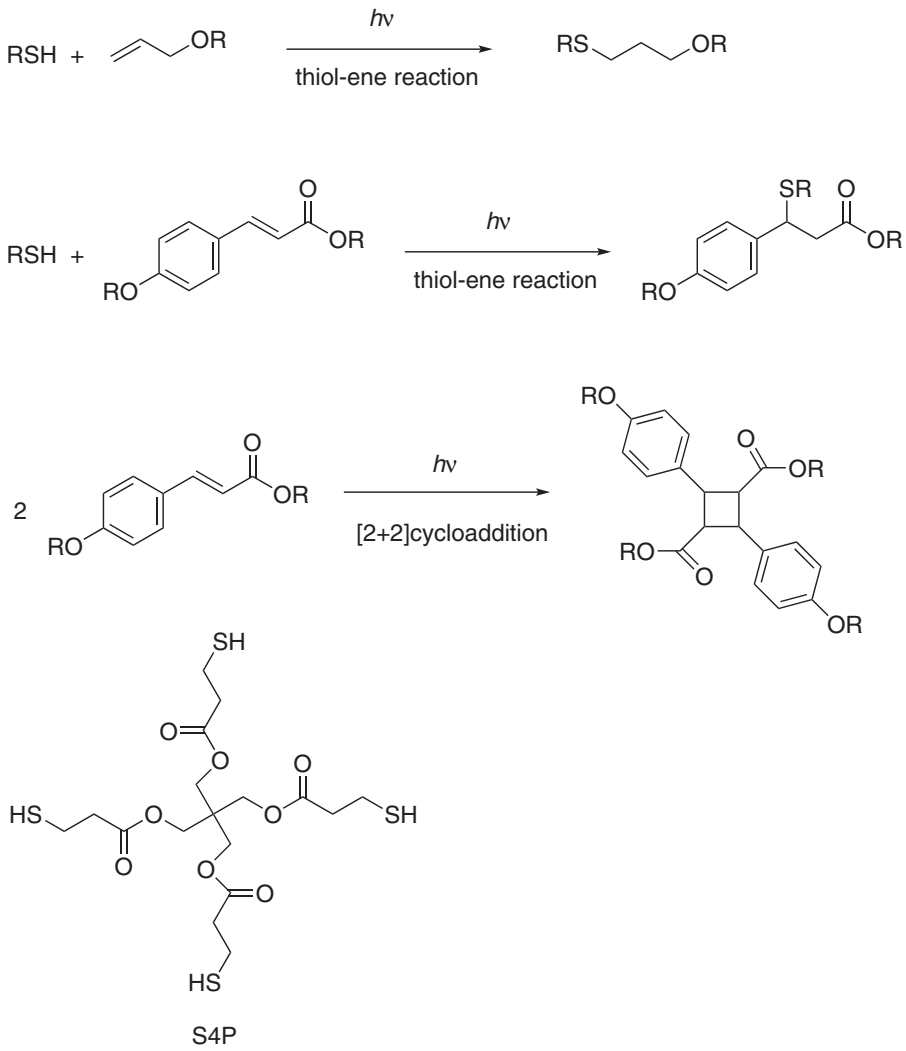

S4P

bromide (3.63 g, 30.0 mmol) and potassium carbonate (4.14 g, 30.0 mmol) in a similar manner to the above to give A3CF as pale yellow crystals (7.82 g) in 52% yield. A3CF: mp. 56.7 °C; ^{13}C-NMR (100 MHz, δ, ppm, in $CDCl_3$) 166.59 (C-1), 150.60 (C-7), 148.47 (C-6), 145.33 (C-3), 134.23, 133.98, 133.36 (C-11, 14, 17), 127.49 (C-4), 123.56 (C-9), 118.23, 117.93, 117.6 (C-12, 15, 18), 115.91 (C-2), 113.80, 112.92 (C-8,5), 69.40, 69.26 (C-13, 16), 64.80 (C-10); ESI-MS (positive mode, *m/z*) calcd. for $C_{18}H_{20}O_4$ 300.1362, found $[M + H]^+$ 301.1430.

[2+2] Photodimerization of A2CM and A3CF

A 23.9 μM acetonitrile solution (10 mL) of A3CF in a quartz cell with a size of $45 \times 10 \times 10$ mm^3 was photo-irradiated for a specified time through a poly(methyl methacrylate) filter, which removed light of wavelengths lower than 280 nm. A SPOT-CURE SP-7 (250 W light source, wavelength 240–440 nm, Ushio Inc., Yokohama, Japan) device equipped with a uniform-radiation optical unit was used for UV curing (irradiation distance 17 cm, irradiation intensity 60 mW cm^{-2}). A 23.9 μM acetonitrile solution (10 mL) of A2CM was similarly photodimerized.

Thiol-ene photopolymerization

A typical procedure for the thiol-ene photopolymerization of A3CF and S4P at a molar ratio of 4/3 is as follows: A mixture of A3CF (2.70 g, 8.99 mmol), S4P (3.30 g, 6.74 mmol), photoinitiators (total 180 mg, 3.0 wt% of the total weight of reactants, IRGACURE® 184 /IRGACURE® 819 = 3/1 (w/w)) was stirred for 1 h to form a homogeneous solution. The solution was poured onto a polymethylpentene culture dish with a diameter of 80 mm and photoirradiated three times for 60 s at 1 min intervals to yield a photocured A3CM/S4P 4/3 film (A3CM-S4P43) with a thickness of 0.2 mm. A SPOT-CURE SP-7 device equipped with a uniform-radiation optical unit was used for UV curing (irradiation distance 17 cm, irradiation intensity 60 mW cm^{-2}). In a similar manner, photocured A3CF/S4P 1/1, A2CM/S4P 2/1 and A2CM/S4P 4/3P films

(A3CF-S4P11, A2CM-S4P21 and A2CM-S4P43, respectively) were prepared.

Characterization

Proton and carbon nuclear magnetic resonance (^{1}H- and ^{13}C-NMR) spectra were recorded on a Bruker Ascend 400 MHz spectrometer (Madison, WI, USA) using $CDCl_3$ as the solvent. Fourier transform infrared (FT-IR) spectra were recorded at room temperature in the range from 4000 to 700 cm^{-1} on a Shimadzu (Kyoto, Japan) IRAffinity-1S by the attenuated total reflectance (ATR) method. The IR spectra were acquired using 50 scans at a resolution of 4 cm^{-1}. Gel fractions were measured by the following procedure: A film ($10 \times 10 \times 0.3$–0.5 mm^3) was submerged in chloroform at room temperature for 24 h, and subsequently, the film was removed and dried at 40 °C in a vacuum oven for 24 h. The gel fraction was calculated by the equation: Gel fraction (%) = 100 w_1/w_0, where w_0 and w_1 are the weights of the original and dried films, respectively. Ultraviolet–visible (UV–Vis) spectra were recorded on a JASCO V-650 instrument (Tokyo, Japan) over the wavelength range of 400 to 800 nm using an acetonitrile solution in a quartz cell. The differential scanning calorimetry (DSC) measurements were performed on a Perkin-Elmer Diamond DSC (Waltham, MA, USA) in a helium atmosphere. To eliminate the thermal history of the samples (5–8 mg), the samples were heated from −50 to 200 °C at a heating rate of 20 °C min^{-1}, held at the temperature for 3 min, and then cooled to −50 °C at a cooling rate of 100 °C min^{-1}. After the temperature was held at −50 °C for 3 min, the second heating scan was performed at a heating rate of 20 °C min^{-1} to determine the glass transition temperature (T_g). The 5% weight loss temperature (T_{d5}) was measured on a Shimadzu TGA-50 thermogravimetric analyzer. A sample of approximately 5 mg was heated from room temperature to 500 °C at a heating rate of 20 °C min^{-1} in a nitrogen purge stream at a flow rate of 50 mL min^{-1}. The tensile testing of rectangular plates (length 50 mm, width 10 mm, and thickness 0.9 mm) was performed at room temperature (ca. 20 °C) using a Shimadzu Autograph AG-1. The span length was 25 mm, and the testing speed was 10 mm min^{-1}. Five specimens were tested for each set of samples, and the mean value and standard deviation were calculated.

Results and discussion

Characterization of A2CM and A3CF

Since the allylation reactions of CMA and CFA using large excess amounts of allyl bromide and potassium carbonate only once produced incompletely allylated products, the fully allylated products (A2CM and A3CF) were synthesized by repeating the reactions using slightly excess amounts of allyl bromide and potassium carbonate (Scheme 1). Figures 1 and 2 show the ^{1}H-NMR spectra of A2CM and A3CF in d_6-DMSO, respectively. The expanded spectra of each signal of A2CM and A3CF are also shown in Figs. S1 and S2 (see Supplementary Materials). In the ^{1}H-NMR spectrum of A2CM, the ^{1}H-signals of the benzene core were observed at δ 7.68 (d, 2H, H-5,9, $J = 8.7$ Hz) and 7.00 ppm (d, 2H, H-6, 8, $J = 8.7$ Hz), and those of the unsaturated carbonyl moiety were at δ 7.64 (d, 1H, H-3, $J = 16.0$ Hz) and 6.52 ppm (d, 1H, H-2, $J = 16.0$ Hz). The ^{1}H-signals of two allyl groups were observed at δ 6.01 (m, 2H, H-11,14), 5.41 (dd, 1H, H-15a or 12a, $J = 18.3$, 1.2 Hz), 5.36 (dd, 1H, H-12a or 15a, $J = 17.8$, 1.2 Hz), 5.28 (d, 1H, H-15b or 12b, $J =$ 11.3 Hz), 5.25 (d, 1H, H-12b or 15b, $J = 10.5$ Hz), 4.67 (d, 1H, H-10, $J = 5.4$ Hz), and 4.62 (d, 1H, H-13, $J =$ 5.2 Hz). In the ^{1}H-NMR spectrum of A3CF, the ^{1}H-signals of the benzene core were observed at δ 7.40 (d, 1H, H-5, $J = 1.6$ Hz), 7.24 (dd, 1H, H-9, $J = 8.4$, 1.6 Hz) and 7.00 ppm (d, 1H, H-8, $J = 8.4$ Hz), and those of the unsaturated carbonyl moiety were at δ 7.60 (d, 1H, H-3, $J = 16.0$ Hz) and 6.58 ppm (d, 1H, H-2, $J = 16.0$ Hz). The ^{1}H-signals of three allyl groups were observed at δ 6.01 (m, 3H, H-11,14,17), 5.46–5.33 (m, 3H, H-15a,18a,12a), 5.25 (m, 3H, H-12b,15b,18b), 4.67 (d, 2H, H-10, $J = 5.5$ Hz), 4.63 (d, 2H, H-13 or 16, $J = 5.7$ Hz), and 4.62 (d, 2H, H-16 or 13, $J = 6.0$ Hz). Furthermore, all the ^{13}C-signals in the ^{13}C-NMR spectra of A2CM and A3CF were reasonably assigned as shown in Figs. S3 and S4 (see Supplementary Materials). The chemical structures of A2CM and A3CF as characterized by the ^{1}H- and ^{13}C-NMR spectral analyses were confirmed by the electrospray ionization mass spectrometry (ESI-MS) analysis (see Materials and methods).

Photopolymerization of A2CM and A3CF with S4P

Figure 3 shows UV–Vis spectral changes of the acetonitrile solutions of A2CM and A3CF, to which light of 280–440 nm was irradiated for 3–30 s. In the case of A2CM, the intensity of the absorption band at 310 nm decreased with irradiation time and became substantially constant at an irradiation time of 12–15 s. Similarly, the intensities of the absorption bands at 295 and 320 nm of A3CM decreased and became constant at an irradiation time of 20–30 s. The fact that both UV–Vis spectral changes had isosbestic points indicates that A2CM and A3CF photodimerized without the generation of byproducts in the diluted acetonitrile solutions (see Fig. S5 in Supplementary Materials). A similar UV spectral change is known for the photodimerization of coumaric acid derivatives [34, 35]. However, when a neat liquid of A2CM was directly UV-irradiated at room temperature for 180 s in a similar manner, the photodimerization did not occur, as is evident

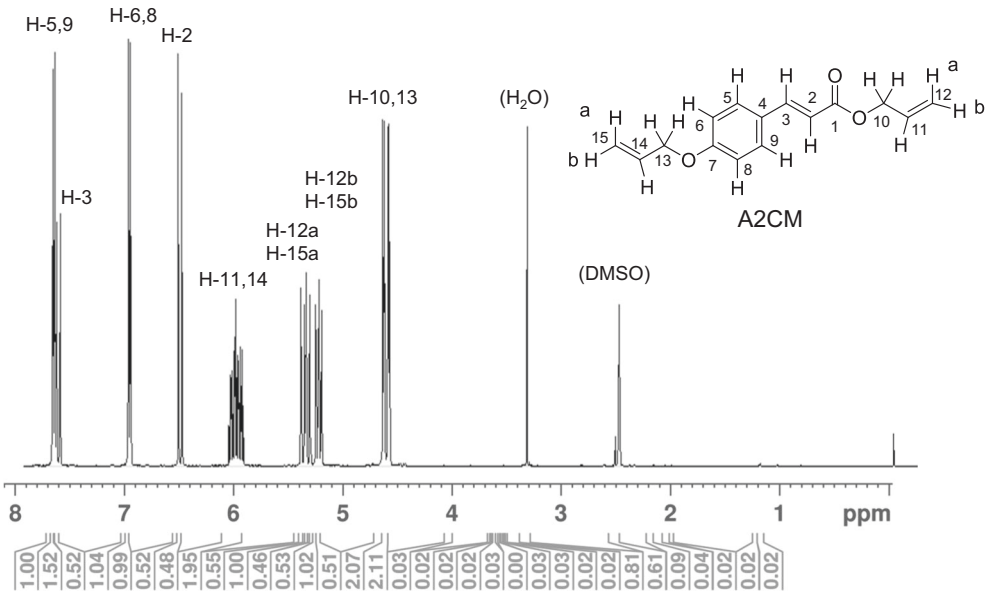

Fig. 1 Four-hundred megahertz ^{1}H-NMR spectrum of A2CM in DMSO-d_6. The red numeric characters indicate the integration of each ^{1}H-signal (color figure online)

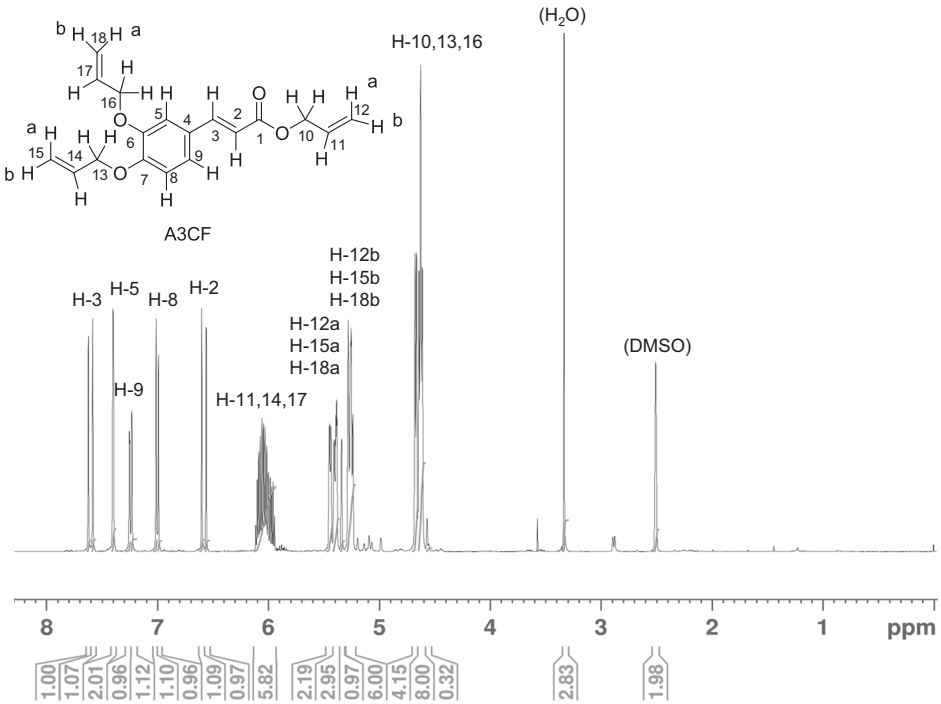

Fig. 2 Four-hundred megahertz ^{1}H-NMR spectrum of A3CF in DMSO-d_6. The red numeric characters indicate the integration of each ^{1}H-signal (color figure online)

from the fact that the ^{1}H-NMR spectrum of the irradiated sample was the same as that of the original A2CM. Similarly, although a melted A3CF at 60 °C was comparably photo-irradiated, no reaction occurred. Therefore, it is presumed that the [2 + 2] dimerization reaction hardly occurs during the photoirradiation of A2CM/S4P or A3CF/S4P without solvent.

Next, the mixtures A2CM/S4P and A3CF/S4P were photocured by the thiol-ene reaction in the presence of photoinitiators at molar ratios of 2/1 and 4/3, that is, an allyl/thiol ratio of 1/1, to yield A2CM-S4P21 and A3CF-S4P43, respectively. The A2CM-S4P21 and A3CF-S4P43 films were obtained as pale yellow and visually transparent films (Fig. 4). Furthermore, assuming that the thiol-ene reaction of the thiol groups of S4P and enone (CH=CHC=O) groups of A2CM and A3CF occurs, the mixtures of A2CM/S4P and A3CF/S4P were photocured at

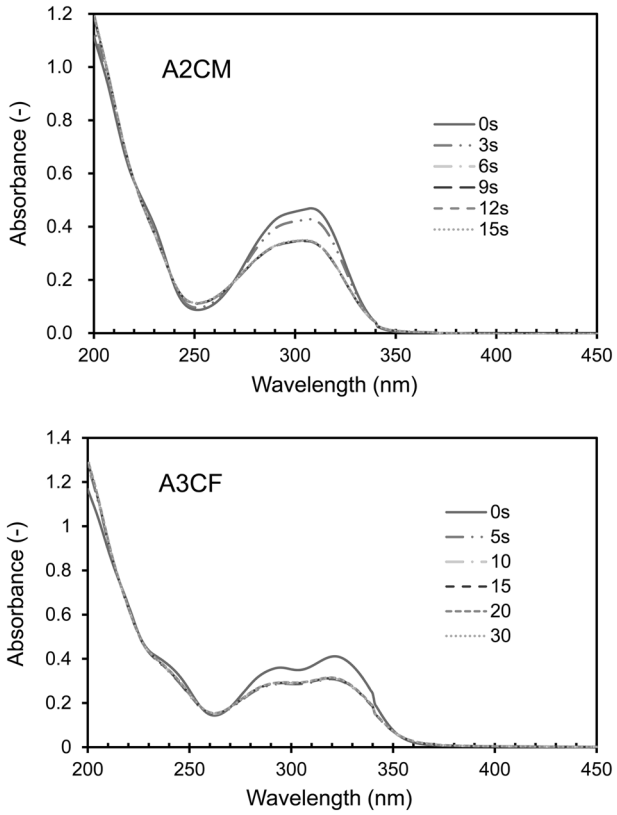

Fig. 3 UV–Vis spectral changes of 23.9 μM acetonitrile solutions of A2CM and A3CF irradiated with light of 280–440 nm for 3–30 s

molar ratios of 4/3 and 1/1, that is an (allyl + enone)/thiol ratio of 1/1, to yield A2CM-S4P43 and A3CF-S4P11, respectively. The A2CM-S4P43 and A3CF-S4P11 films were also pale yellow and visually transparent.

Figure 5 shows the FT-IR spectra of all the photocured films and their reactants. S4P displayed an intense band due to the ester carbonyl stretching vibration ($\nu_{C=O}$) at 1726 cm^{-1} and a weak absorption band due to the stretching vibration of the S-H group (ν_{SH}) at 2563 cm^{-1}. The ν_{SH} band was apparent in a longitudinally enlarged spectrum of the wavelength region from 2400 to 2700 cm^{-1}. A2CM exhibited an unsaturated ester $\nu_{C=O}$ band at 1707 cm^{-1} and bands ascribed to C=C stretching ($\nu_{C=C}$) and = C–H out-of-plane bending ($\gamma_{=C-H}$) vibrations at 1631 cm^{-1} and 986, 926 cm^{-1}, respectively. Additionally, A3CF exhibited an unsaturated ester $\nu_{C=O}$ band at 1705 cm^{-1}, $\nu_{C=C}$ bands at 1649 and 1628 cm^{-1}, and $\gamma_{=C-H}$ bands at 981 and 920 cm^{-1}. The $\nu_{C=C}$ bands at 1628–1649 cm^{-1} for A2CM and A3CF are ascribed to the C=C bonds of allyl and enone groups [23, 25, 34]. It is known that the allyloxy $\gamma_{=C-H}$ band is observed as two peaks at approximately 995–985 cm^{-1} and 915–905 cm^{-1} [23, 24], and the *trans*-vinylene $\gamma_{=C-H}$ band of a cinnamoyl group is observed as one peak at approximately 980 cm^{-1} [36]. Therefore, the peaks at 926 and 920 cm^{-1} are ascribed to the allyl groups, and those at 986 and 981 cm^{-1} are ascribed to both the allyl and *trans*-enone groups in the FT-IR spectra of A2CM and A3CF, respectively. In the FT-IR spectra of A2CM-S4P21 and A3CF-S4P43, the ν_{SH} band was nonexistent, and the allyl $\gamma_{=C-H}$ band at approximately 926–920 cm^{-1} was considerably weaker than those of A2CM and A3CF. It is considered that the residual band at approximately 926–920 cm^{-1} may be attributed to the absorption band of S4P because S4P has a weak absorption band at 934 cm^{-1}. These results indicate that the thiol-ene reaction of allyl and thiol groups almost completely progressed for A2CM-S4P21 and A3CF-S4P43. These cured products displayed relatively intense peaks at 1670 and 1662 cm^{-1}, respectively, which were at a slightly higher wavenumber region than the $\nu_{C=C}$ bands of the enone groups of A2CM and A3CF (1628–1649 cm^{-1}). These peaks are considered to be $\nu_{C=C}$ bands of the distorted enone moieties in which the conjugation of C=C and C=O bonds is disturbed by the thiol-ene crosslinking reaction of allyl and thiol groups. The fact that the peak intensity of the band at 1662 cm^{-1} for A3F-S4P43 is much higher than that of the band at 1670 cm^{-1} for A2CM-S4P21 may be attributed to the factor that the enone conjugation of A3F-S4P43 is much more disturbed by a highly crosslinked structure, leading to a nonplanar conformation. Thus, it is considered that the allyl groups of A2CM and A3CF have a higher thiol-ene reactivity than do the enone groups, and the C=C bonds of the enone groups of A2CM and A3CF hardly reacted with the thiol groups of S4P. As a similar reaction behavior, it is known that allyl groups have a higher thiol-ene reactivity than that of acrylate and methacrylate groups [10]. In the FT-IR spectra of A2CM-S4P43 and A3CF-S4P11, the ν_{SH} band was nonexistent, and the allyl $\gamma_{=C-H}$ bands at 981 and 920 cm^{-1} were considerably diminished in a similar manner to those A2CM-S4P21 and A3CF-S4P43. Unlike the case of A2CM-S4P21 and A3CF-S4P43, A2CM-S4P43 and A3CF-S4P11 displayed no $\nu_{C=C}$ band at approximately 1660–1670 cm^{-1}. These results indicate that the thiol-ene reaction of the thiol groups of S4P with the alkenyl groups of allyl and enone groups almost completely proceeded for A2CM-S4P43 and A3CF-S4P11. However, in the FT-IR spectrum of A2CM-S4P43, an unsaturated ester $\nu_{C=O}$ band was observed as a shoulder peak at 1705 cm^{-1}, and weak $\nu_{C=C}$ and allyloxy $\gamma_{=C-H}$ bands appeared at 1632 and 926 cm^{-1}, respectively. This result indicates that some amounts of allyl and enone groups remained in A2CM-S4P43. It is considered that, in addition to the allyl groups, the thiol groups of S4P also reacted with the enone groups of A2CM-S4P43 with a (allyl + enone)/thiol ratio of 1/1, in contrast to the selective reaction of thiol and allyl groups for A2CM-S4P21 with an allyl/thiol ratio of 1/1 and that the thiol-ene reaction of the residual allyl and

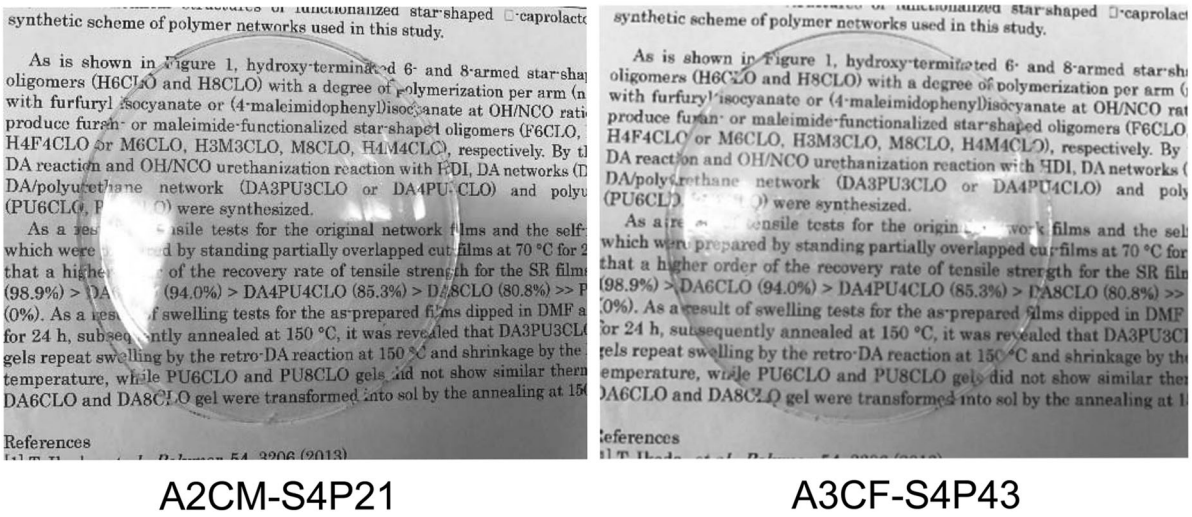

Fig. 4 Photographs of A2CM-S4P21 and A3CF-S4P43 films

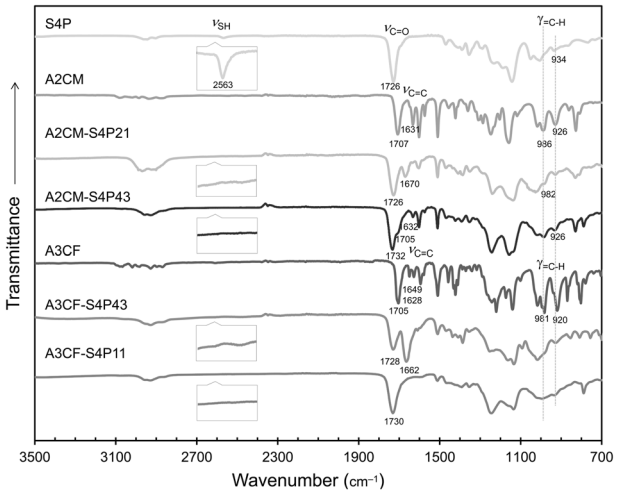

Fig. 5 FT-IR spectra of all the cured products compared with those of S4P, A2CM, and A3CF

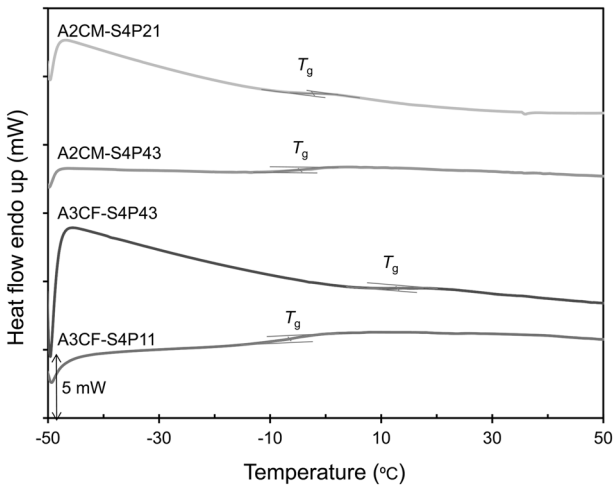

Fig. 6 DSC curves of all the cured products

enone groups was disturbed by the formation of a highly crosslinked network at the final stage of curing for A2CM-S4P43. In fact, the gel fraction (90%) of A2CM-S4P43 was slightly lower than that (92%) of A2CM-S4P21. In a similar trend, the gel fraction (81%) of A3CF-S4P11 was lower than that (87%) of A3CF-S4P43. Additionally, the gel fractions of A3CF-S4P43 and A3CF-S4P11 were lower than those of A2CM-S4P21 and A2CM-S4P43, respectively. These results are in accordance with the fact that the conversion at a gelation point decreases with increasing monomer functionalities, as based on the Flory-Stockmayer theory. Although we could not detect the presence of residual allyl, enone and thiol groups by the ATR-IR surface analysis of A2CM-S4P21, A3CF-S3P43 and A3CF-S4P11, there is a possibility that some functional groups remain in the inner region of the films.

Thermal and mechanical properties of cured products

Figure 6 shows the DSC curves of all the photocured products. The T_g (13.2 °C) of A3CF-S4P43 was substantially higher than that (–7.2 °C) of A3CF-S4P11 (Table 1). This result may be caused by the facts that rigid cinnamate moieties were retained for A3CF-S4P43, whereas the original enone group of A3CF was converted to a saturated carbonyl group for A3CF-S4P11 by the thiol-ene reaction and that S4P feed weight fraction (55.0 wt%) of A3CF-S4P43 was lower than that (61.9 wt%) of A3CF-S4P11, considering that S4P is a flexible aliphatic thiol compound. Furthermore, the T_g (–2.8 °C) of A2CM-S4P21 was slightly higher than that (–4.6 °C) of A2CM-S4P43 due to the same reasons as the case of A3CF-S4P43 and A3CF-S4P11. However, the difference in T_g was very small. This result is

Table 1 Composition, T_g and T_{d5} of all the photocured products

Sample	Feed molar ratio	Feed weight fraction of S4P (wt%)	Average functionality of feed monomers (-)	T_g (°C)	T_{d5} (°C)
A2CM-S4P21	A2CM/S4P = 2/1[a]	50.0	(3×2 + 4 × 1)/3 ≅ 3.33	–2.8	336
A2CM-S4P43	A2CM/S4P = 4/3[b]	60.0	(3×4 + 4 × 3)/7 ≅ 3.43	–4.6	334
A3CF-S4P43	A3CF/S4P = 4/3[a]	55.0	(4×4 + 4 × 3)/7 = 4.00	13.2	377
A3CF-S4P11	A3CF/S4P = 1/1[b]	61.9	(4×1 + 4 × 1)/2 = 4.00	–7.2	342

[a]Allyl/thiol = 1/1

[b](Allyl + enone)/thiol = 1/1

attributable to the fact that the average feed monomer functionality (3.33) of A2CM-S4P21 was slightly lower than that (3.43) of A2CM-S4P43, leading to a lower crosslinking density of A2CM-S4P21 (Table 1). Therefore, it is considered that the T_g of this curing system depends on the content of flexible alkylene moieties in addition to the crosslinking density.

Figure 7 shows the TGA curves of all the photocured products. The T_{d5}s of A3CF-S4P43 and A3CF-S4P11 were higher than those of A2CM-S4P21 and A2CM-S4P43, respectively (Table 1). This result should be caused by the fact that the average feed monomer functionalities (4.00) of A3CF-S4P43 and A3CF-S4P11 were higher than those (3.33 and 3.43) of A2CM-S4P21 and A2CM-S4P43, respectively (Table 1). Additionally, the T_{d5}s of A2CM-S4P21 and A3CF-S4P43, in which enone groups remain, were higher than those of A2CM-S4P43 and A3CF-S4P11, in which the enone (–CH=CH–C(=O)O–) moieties were converted to saturated thioester (–(RS)CH–CH_2–C(=O)O–) moieties, respectively (Table 1). This result may be related to the fact that thiol (RSH) groups are apt to eliminate thermally from saturated thioester moieties. As a result, A3CF-S4P43 exhibited the highest T_{d5} (377 °C) among all the cured products.

Figure 8 shows the stress–strain curves of all the cured products. Furthermore, the values of tensile strength, modulus and elongation at break are shown in Fig. 9. A3CF-S4P43, with the highest T_g (14.0 °C), exhibited the highest tensile strength and modulus among all the cured products. However, A3CF-S4P11, with the lowest T_g (–4.9 °C), displayed the lowest tensile strength and modulus. These results should be related to the factors that A3CF-S4P43 is in a glassy/rubbery transition state due to a very broad glass transition behavior at approximately 5–20 °C and that A3CF-S4P11 is in a rubbery state at the testing temperature of approximately 20 °C. The fact that A3CF-S4P11 displayed the lowest elongation at break should be caused by the highest crosslinking density, as estimated from the highest average functionality (4.00) of feed monomers and stoichiometric reaction at (allyl + enone)/thiol = 1/1. Although we do not know a clear reason for the fact that A3CF-S4P43 in a glassy/rubbery transition state exhibited

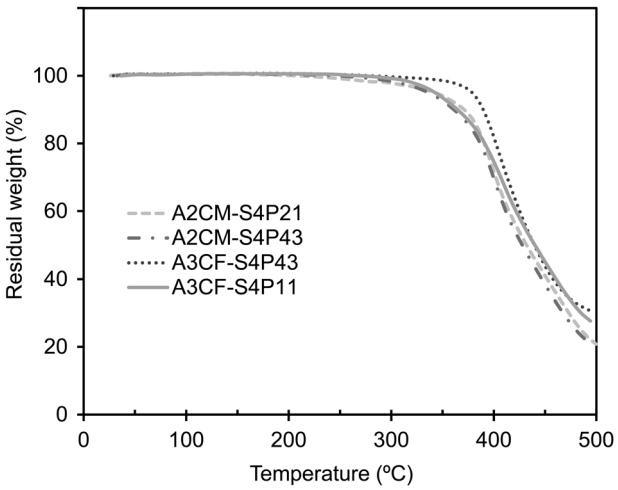

Fig. 7 TGA curves of all the cured products

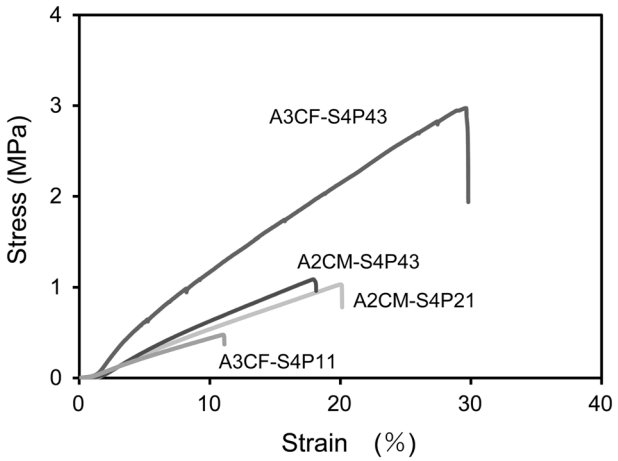

Fig. 8 Stress–strain curves of all the cured products

the highest elongation at break, the nonplanar structure due to a disturbance of the enone conjugation may facilitate chain entanglement, as discussed in the FT-IR section. As A2CM-S4P21 and A2CM-S4P43 with comparable T_gs (–1 to –2 °C) are also in a rubbery state at the testing temperature, the tensile properties of these cured products were comparable to each other and were significantly worse than those of A3CF-S4P43.

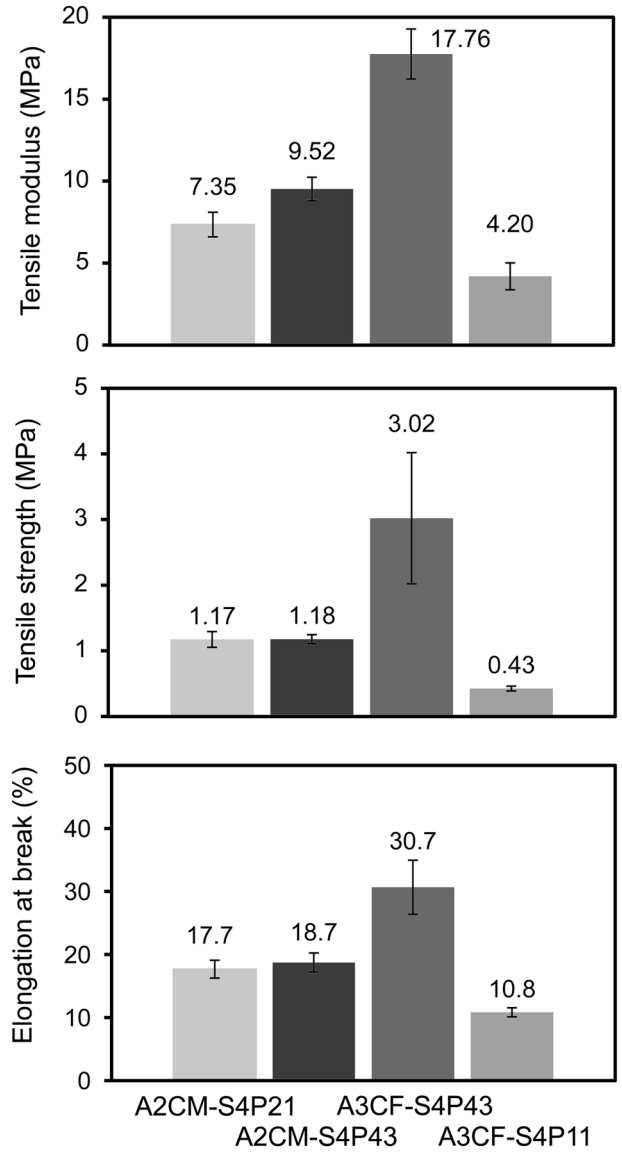

Fig. 9 Tensile strengths, moduli, and elongations at break of all the cured products

Conclusions

A2CM and A3CF were synthesized by the allylation reaction of CMA and CFA, respectively, and the thermal and mechanical properties of their photocured products with S4P were investigated in relation to the products of the thiol-ene reaction of the allyl and enone groups of A2CM and A3CF and the thiol groups of S4P, as well as to that of the [2 + 2] photodimerization reaction of A2CM and A3CF. A2CM and A3CF did not photodimerize without a solvent, even though their compounds photodimerized in dilute acetonitrile solutions. When A2CM and A3CF were photocured with S4P at an allyl/thiol ratio of 1/1, the thiol-ene reaction of allyl and thiol groups selectively occurred to produce A2CM-S4P21 and A3CF-S4P43. A3CF-S4P43 exhibited a higher T_g and T_d than A2CM-S4P21. When A2CM and A3CF were photocured with S4P at an (allyl + enone)/thiol ratio of 1/1, both the thiol-ene reactions of the allyl/thiol and enone/thiol groups occurred to produce A2CM-S4P43 and A3CF-S4P11. The FT-IR analysis showed that almost all the allyl and enone groups were consumed for A3CF-S4P11, whereas some amounts of allyl and enone groups remained for A2CM-S4P43. The progress of the thiol-ene reaction of enone and thiol groups as well as an increase in the S4P feed content caused the lowering of T_g and T_{d5}. As a result, A3CF-S4P43, in which rigid cinnamate moieties are held, exhibited the highest T_g, T_{d5} and tensile properties among all the cured products. A3CF is a promising biobased monomer for thiol-ene photocuring resin systems.

Acknowledgements We thank Dr. Naozumi Teramoto and Dr. Toshiaki Shimasaki of our department for their helpful suggestions.

Compliance with ethical standards

Conflict of interest The authors declare that they have no conflict of interest.

Publisher's note: Springer Nature remains neutral with regard to jurisdictional claims in published maps and institutional affiliations.

References

1. Spierling S, Knüpffer E, Behnsen H, Mudersbach M, Krieg H, Springer S, et al. Bio-based plastics–A review of environmental, social and economic impact assessments. J Clean Prod. 2018;185:476–91.
2. Lambert S, Wagner M. Environmental performance of bio-based and biodegradable plastics: the road ahead. Chem Soc Rev. 2017;46:6855–71.
3. Kristufek SL, Wacker KT, Tsao YT, Su L, Wooley KL. Monomer design strategies to create natural product-based polymer materials. Nat Prod Rep. 2017;34:433–59.
4. Gandini A, Lacerda TM, Carvalho AJF, Trovatti E. Progress of polymers from renewable resources: Furans, vegetable oils, and polysaccharides. Chem Rev. 2016;116:1637–69.
5. Gandini A, Lacerda TM. From monomers to polymers from renewable resources: Recent advances. Prog Polym Sci. 2015;48:1–39.
6. Baroncini EA, Stanzione JF III. Incorporating allylated lignin-derivatives in thiol-ene gel-polymer electrolytes. Int J Biol Macromol. 2018;113:1041–51.
7. Resetco C, Hendriks B, Badi N, Prez FD. Thiol–ene chemistry for polymer coatings and surface modification – building in sustainability and performance. Mater Horiz. 2017;4:1041–53.
8. Machado TO, Sayer C, Araujo PHH. Thiol-ene polymerisation: A promising technique to obtain novel biomaterials. Eur Polym J. 2017;86:200–15.
9. Lowe AB. Thiol-ene "click" reactions and recent applications in polymer and materials synthesis: a first update. Polym Chem. 2014;5:4820–70.
10. Lowe AB. Thiol-ene "click" reactions and recent applications in polymer and materials synthesis. Polym Chem. 2010;1:17–36.

11. Zhang D, Liang H, Bu J, Xiong L, Huang S, Zhang DD, et al. UV curable soybean-oil hybrid systems based on thiol-acrylate and thiol-ene-acrylate chemistry. J Appl Polym Sci. 2015;132:42095.
12. Echeverri DA, Cádiz V, Ronda JC, Rios LA. Synthesis of elastomeric networks from maleated soybean-oil glycerides by thiol-ene coupling. Eur Polym J. 2012;48:2040–9.
13. Luo A, Jiang X, Lin H, Yin J. "Thiol-ene" photo-cured hybrid materials based on POSS and renewable vegetable oil. J Mater Chem. 2011;21:12753–60.
14. Black M, Rawlins JW. Thiol-ene UV-curable coatings using vegetable oil macromonomers. Eur Polym J. 2009;45:1433–41.
15. Ortiz RA, Martinez AYR, Valdéz AEG, Duarte MLB. An effective method to prepare sucrose polymers by thiol-ene photopolymerization. Carbohydr Polym. 2009;78:282–6.
16. Ortiz RA, Martinez AYR, Valdéz AEG, Duarte MLB. Preparation of a crosslinked sucrose polymer by thiol-ene photopolymerization using dithiothreitol as comonomer. Carbohydr Polym. 2010;82:822–8.
17. Nagashima S, Shimasaki T, Teramoto N, Shibata M. Trehalose-incorporated polymer network by thiol-ene photopolymerization. Polym J. 2014;46:728–35.
18. Shibata M, Nagashima S. Trehalose-incorporated organic–inorganic hybrid nanocomposites produced by thiol-ene photopolymerization. Polym J. 2015;48:111–6.
19. Li C, Johansson M, Sablong RJ, Koning CE. High performance thiol-ene thermosets based on fully bio-based poly(limonene carbonate)s. Eur Polym J. 2017;96:337–49.
20. Oritiz RA, Blandón EAO, Santos RG. Synthesis of novel hexathiolated squalene and its thiol-ene photopolymerization with unsaturated monomers. Green Sustain Chem. 2012;2:62–70.
21. Yokose R, Shimasaki T, Teramoto N, Shibata M. Amino acid-incorporated polymer network by thiol-ene polymerization. Express Polym Lett. 2015;9:744–55.
22. Aoyagi S, Shimasaki T, Teramoto N, Shibata M. Bio-based polymer networks by thiol-ene photopolymerization of allylated L-glutamic acids and L-tyrosines. Eur Polym J. 2018;101:151–8.
23. Yoshimura T, Shimasaki T, Teramoto N, Shibata M. Bio-based polymer networks by thiol-ene photopolymerizations of allyletherified eugenol derivatives. Eur Polym J. 2015;67:397–408.
24. Modjinou T, Versace DL, Abbad-Andallousi S, Bousserrhine N, PDubot P, Langlois V, et al. Antibacterial and antioxidant bio-based networks derived from eugenol using photo-activated thiol-ene reaction. React Funct Polym. 2016;101:47–53.
25. Uemura Y, Shimasaki T, Teramoto N, Shibata M. Thermal and mechanical properties of bio-based polymer networks by thiol-ene photopolymerizations of gallic acid and pyrogallol derivatives. J Polym Res. 2016;23:216.
26. Yang G, Kristufek SL, Link LA, Wooley KL, Robertson ML. Synthesis and physical properties of thiol-ene networks utilizing plant-derived phenolic acids. Macromolecules. 2015;48:8418–27.
27. Yang G, Kristufek SL, Link LA, Wooley KL, Robertson ML. Thiol-ene elastomers derived from biobased phenolic acids with varying functionality. Macromolecules. 2015;49:7737–48.
28. Taofiq O, González-Paramás AM, Barreiro MF, Ferreira ICFR. Hydroxycinnamic acids and their derivatives:Cosmeceutical significance, challenges and future perspectives, a review. Molecules. 2017;22:281.
29. Sun J, Lin Y, Shen X, Jalin R, Sun X, Yuan Q, et al. Aerobic biosynthesis of hydrocinnamic acids in *Escherichia coli* with a strictly oxygen-sensitive enoate reductase. Metab Engn. 2016;35:75–82.
30. Rodrigues JL, Araújo RG, Prather KLJ, Kluskens LD, Rodrigues LR. Heterologous production of caffeic acid from tyrosine in *Escherichia coli*. Enzym Microb Technol. 2015;71:36–44.
31. Furuya T, Arai Y, Kino K. Biotechnological production of caffeic acid by bacterial Cytochrome P450 CYP199A2. Appl Ebviron Microbiol. 2012;78:6087–94.
32. Sidoryk K, Jaromin A, Filipczak N, Cmoch P, Cybulski M. Synthesis and antioxidant activity of caffeic acid derivatives. Molecules. 2018;23:2199.
33. Poplata S, Tröster A, Zou YQ, Bach T. Recent advances in the synthesis of cyclobutanes by olefin [2+2] photocycloaddition reactions. Chem Rev. 2016;116:9748–815.
34. Benˇová E, Zeleňánk V, Halamová D, Almaˊši M, Petrul'ová V, Psotka M, et al. A drug delivery system based on switchable photo-controlled *p*-coumaric acid derivatives anchored on mesoporous silica. J Mater Chem B. 2017;5:817–25.
35. Chae B, Lee SW, Ree M, Jung YM, Kim SB. Photoreaction and molecular reorientation in a nanoscale film of poly(methyl 4-(methacryloyloxy)cinnamate) studied by two-dimentional FTIR and UV correlation spectroscopy. Langmuir. 2003;19:687–95.
36. Currie DJ, Lough CE, McClusky FK, Holmes HL. Effect of functional group conformation on the infrared spectra of some gem difunctional phenylethylene derivatives. Can J Chem. 1969;47:3147–52.